Chapter 12
Resolving Internal and Global Dynamics of Proteins by Combination of Time-Resolved Fluorescence Anisotropy and Fluorescence Correlation Spectroscopy

Labe A. Black and J. B. Alexander Ross

Keywords Protein dynamics · Time-resolved fluorescence anisotropy · Fluorescence correlation spectroscopy · Diffusion · Global analysis

12.1 Introduction

Fluorescence methods are able to resolve dynamic motion timescales that range from picoseconds to seconds or longer and allow the determination of molecular and cellular dynamics under similar data collection conditions with minimal chemical modifications [1, 3–6]. However, depending on the fluorescence method used to assess the timescales of the motions of interest, the parameters recovered from the data analysis may be ill determined. For example, the timescales for local and other internal motions of proteins can vary from picoseconds for sidechain rotations to milliseconds for domain motions (e.g., opening and closing). In an aqueous, unrestricted environment, the whole-molecule rotation for globular proteins scale with the molecular weight (on the order of a half nanosecond per kDa at ambient temperature (~20 °C) [7–9]) and can be orders of magnitude slower than local motions. As will be discussed, the difference in timescales for these motions, compared with the excited-state lifetime of the probes used to measure them, can complicate accurate determination and resolution of the different kinds of motion.

Time-resolved fluorescence anisotropy (TRFA) is a well-established method for measuring rotational diffusion and internal motions of proteins. As discussed by Lakowicz [8], the observed value of the time-average or steady-state anisotropy depends on three factors. First is the mean correlation time (ϕ) due to many dynamic motions, which depends on size and shape of the macromolecule (or assembly),

L. A. Black · J. B. Alexander Ross (✉)
Department of Chemistry and Biochemistry, University of Montana, Missoula, MT, USA
e-mail: sandy.ross@umontana.edu

C. D. Geddes (ed.), *Reviews in Fluorescence 2017*, Reviews in Fluorescence,
https://doi.org/10.1007/978-3-030-01569-5_12

internal dynamics, and single-bond rotations of the probe linker. Second is the fluorescence lifetime (τ) of the probe, which depends on photophysics and interactions with the local environment. Third is the time-zero or limiting anisotropy (r_0), which is determined by the angle between the probe's absorption and emission transition dipoles.

The challenge and potential limitation in using TRFA for accurate determination of any picosecond-to-nanosecond motion is illustrated by the simplest case in which fluorescence lifetime and rotational correlation time are single exponentials. According to the Perrin equation,

$$r = \frac{r_0}{1 + \tau/\phi}, \tag{12.1}$$

where the maximum of the steady-state anisotropy, r, is limited by the absolute value of r_0—the value of r_0 ranges from 0.4 to −0.2 depending on whether the transition dipole moments tend toward parallel or perpendicular alignment with respect to one another—and the observed value of r is then determined by the τ/ϕ ratio. For a given fluorescence lifetime, the rate of molecular rotational motion governs τ/ϕ. In the limit of slow rotational motion (ϕ much longer than τ), the τ/ϕ ratio approaches zero and r approaches r_0. In the limit of fast rotational motions (τ much longer than ϕ), the τ/ϕ ratio becomes very large and r tends toward zero. Thus, the τ/ϕ ratio is a critical consideration for observation of the dynamics of interest. The useful time range for measuring rotational correlation times by TRFA may extend from ~0.1 to 10 times the average lifetime, $<\tau>$ [10], which is an intensity weighted average [11],

$$< \tau >= \int_0^\infty tI(t)dt / \int_0^\infty I(t)dt = \sum_{i=1}^{n} \alpha_i \tau_i^2 / \sum_{i=1}^{n} \alpha_i \tau_i, \tag{12.2}$$

where $I(t)$ represents the intensity decay of the fluorescence probe following excitation, and α_i and τ_i are the amplitude and lifetime, respectively, of the ith intensity decay component.

This review shows how accurate assessment of the times for internal dynamics by TRFA can be facilitated by including independent information about global motion from fluorescence correlation spectroscopy (FCS). Specifically, FCS is used to measure the translational diffusion coefficient of the probe-labelled protein under the same experimental conditions—concentration, solvent, temperature—as those used for TRFA measurements. Then, the FCS-determined translational diffusion coefficient is used to estimate the rotational diffusion coefficient through the Stokes-Einstein-Debye relationship [1, 8, 12]. The value obtained then permits the independent calculation of the global rotational correlation time, which can be used to provide a constraint in the TRFA data analysis; this constraint helps break the cross-correlation between pre-exponential terms and rotational correlation decay terms, inherent in fitting a multi-exponential anisotropy decay model.

12.2 Theoretical Considerations and Analysis Model

The TRFA decay kinetics of an immobile probe attached to an ellipsoidal rotating body can be described by five exponential terms [13–15],

$$r(t) = \sum_{j=1}^{j=5} \beta_j e^{-t/\phi_j}, \tag{12.3}$$

where the pre-exponential factors, β_j, are trigonometric functions of the angles between the excitation and emission transition dipole moments of the probe and the symmetry axes of an ellipsoid [16] (see Fig. 12.1). However, three correlation times at most can be resolved, which is due to two pairs being essentially degenerate [17].

The global rotation of many soluble, globular proteins may adequately be described by a single, mean correlation time [8].

$$\langle \phi \rangle = \left[\frac{\sum \beta_j / \phi_j}{\sum \beta_j} \right]^{-1}. \tag{12.4}$$

In addition, local motions within the protein containing the probe can contribute to additional depolarization, requiring the anisotropy decay, $r(t)$, to be fit as a sum of exponentials that would yield at least two correlation times, ϕ_{short} and ϕ_{long}.

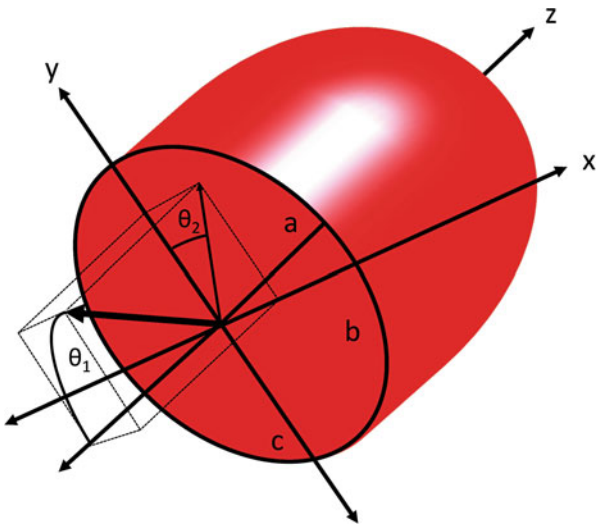

Fig. 12.1 Representation of a general ellipsoid (after Waxman et al. [2]). The semi-axes are $a \geq b \geq c$. It is assumed that the absorbance and emission transition dipole moments of the fluorophore represented by the bold arrow, are coincident. θ_1 and θ_2 are the angles defining the orientation of the dipole moments with respect to the molecular axes. θ_1 is the angle to the major semi-axis a, and θ_2 is defined by the projection onto the plane of the a and c semi-axes.

Accordingly,

$$r(t) = r_0\left[p\, e^{\frac{-t}{\phi_{short}}} + (1-p)e^{\frac{-t}{\phi_{long}}}\right], \tag{12.5}$$

where p is a weighting factor between 0 and 1, and r_0 is the "frozen" or limiting anisotropy at time zero; $r_0\,(1-p) = \beta_{\,long}$ and $r_0 p = \beta_{\,short}$. The longer rotational correlation time is due to the overall rotational motion of the protein, the global rotation (ϕ_{global}), and the shorter rotational correlation time is from both the local (ϕ_{local}) and global motions:

$$\phi_{short}^{-1} = \phi_{local}^{-1} + \phi_{global}^{-1}; \phi_{long}^{-1} = \phi_{global}^{-1}. \tag{12.6}$$

The wobble-in-a-cone model [18] and the order parameter, S^2 [8, 19], have been commonly used to model segmental motions from TRFA data; we have employed both [1, 5]. The wobble-in-a-cone model assumes that the anisotropy component with amplitude $\beta_{\,short}$ reflects motions of the probe within a cone-shaped volume defined by an angle θ with respect to the symmetry axis of the cone; the order parameter, S^2 ranges from 0 for unrestricted motion ($\theta = 90°$) *to 1.0 at complete immobilization* ($\theta = 0°$). Smaller cone angles imply greater local restriction and, conversely, larger cone angles imply greater range of motion. The order parameter and cone angles are obtained using the relationship

$$S^2 = \frac{\beta_{long}}{r_0} = \left[\frac{1}{2}\cos\theta(1 + cos\ \theta)\right]^2, \tag{12.7}$$

where r_0 is the sum of $\beta_{\,short} + \beta_{\,long}$, the amplitudes of the short and long correlation times, respectively.

12.3 A Dynamic Model Protein System

The system used here to test the feasibility of incorporating FCS data into the analysis of TRFA data is the alpha subunit of heterotrimeric G proteins, Gαi1 Hexa I, which is a ~41 kDa protein. Gαi1 Hexa I is a surface cysteine-free construct [20] in which we subsequently incorporated non-native cysteine residues, via site-directed mutagenesis, for covalent attachment of fluorescent probes using cysteine/maleimide chemistry (see Fig. 12.2).

The local dynamics were probed and compared in Gαi1 Hexa I while bound to either nucleotide (GDP or GTPγS) or the chaperone/nucleotide exchange factor Ric-8A, a soluble, cytosolic 60-kDa protein that exhibits specificity for the i, q and

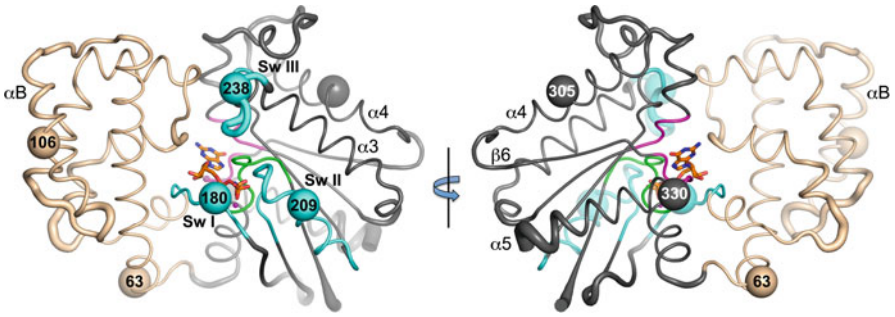

Fig. 12.2 Ribbon schematic of the tertiary structure of Gαi1•GppNHp (PDB ID 1CIP) from Black et al. [1]. The α-helical and Ras-like domains are colored beige and charcoal, respectively. Switch (Sw I-III) segments are colored cyan and labeled. The P-loop and purine binding segments are colored cyan and magenta, respectively. Secondary structure elements of interest are labeled. Alexa 488 (C5) conjugated residues are shown as spheres and labeled

12/13 classes of Gα subunits and accelerates the rate of nucleotide exchange *in vitro* [1].

The TRFA decay of this system requires an accurate determination of the rotational correlation times to resolve local dynamics that involve protein secondary structural changes, amino acid side-chain movements, probe-chain linker and probe-head dynamics. The dynamics of this system is complicated due to multi-exponential TRFA decay components of the fluorescence probe and the overlapping timescales of the local motions. In addition, the instrument used for data acquisition has a resolution of 35 ps/channel, which puts a lower-bound on the timescales that are observable [5]. Consequently, our treatment of the local dynamics includes all collective motion in the local area of the fluorescent probe and which are termed "local" motions.

Local motions in the range of tens of picoseconds to a couple of nanoseconds are unresolvable in our experimental system. The timescale of global rotational motion is five-to-ten times slower for globular proteins within the molecular weight range of 10–100 kDa. Alexa 488, used in these experiments, has a fluorescence lifetime of about four nanoseconds, which is useful for determination of local motions, but progressively less satisfactory for resolution of global motion when molecular weights exceed 50 kDa. With the aid of FCS, however, the global rotational correlation time can be resolved independently from the contributions of the local motions. An important advantage is that FCS and TRFA require chemical modification of only a single point mutation with a single probe, and this allow measurement of the identical sample under the identical experimental conditions—buffer, temperature, concentration—when using different fluorescent methods. This approach facilitates direct comparison of the local motions of our system in its various binding states (nucleotide- and Ric-8A-bound).

12.4 Fluorescence Correlation Spectroscopy

12.4.1 FCS Data Collection

Data acquisition was carried out with an inverted-confocal Olympus IX71 microscope using a 60X 1.2-NA water-objective and 468-nm pulsed-diode laser (20–60 μW, 20 MHz Model LDH-P-C-470 PicoQuant GmbH, Berlin) for excitation. Emission was routed to avalanche photodiodes (APD) (Perkin-Elmer model SPCM-AQR-14-FC) by a 535/50-nm bandpass filter (Chroma Technology Corp., Bellows Falls, VT). The confocal optical train was optimized by obtaining the highest molecular brightness (counts^{-1} molecule^{-1} sec^{-1}) of the Alexa 488 (C5) β-ME adduct. The confocal volume was calibrated using a translational diffusion coefficient of Alexa 488 dye, 420 ± 5 μm^2 s^{-1} at 21.5 °C (value and range calculated from the literature [21–23]). Figure 12.3a is the normalized fluorescence autocorrelation signal for Gαi1 Hexa I with the c-terminal residue 330 mutated to a cysteine and then reacted with Alexa 488 (C5) maleimide (Ax330) bound to GDP or Ric-8A. Figure 12.3b shows the residuals from the single-species fits.

For collection of FCS data, probe-labeled protein complexes were diluted to concentrations of 50–100 pM in the presence of saturating amounts of binding partner (100 μM GDP, 1.5 μM Ric-8A or 10 μM GTPγS). The samples (~1 mL) were placed in a cylindrical confocal microscope sample chamber fitted with optical grade disposable cover slips. SymPhoTime v5.3.2.2 (PicoQuant GmbH, Berlin) software was used both for data acquisition and analysis.

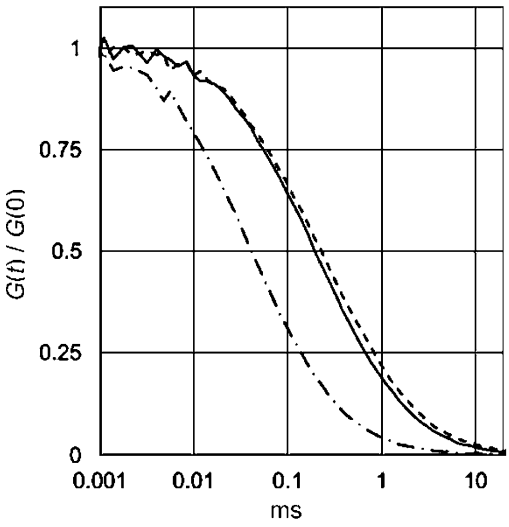

Fig. 12.3a Normalized FCS curves for Ax330 Gαi1:Ric-8A (----), Ax330 Gαi1•GDP (—), and Alexa 488 β-ME adduct (- • - • -). (From Black et al. [1])

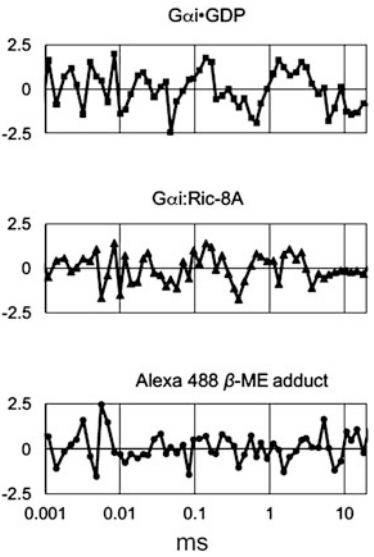

Fig. 12.3b The residuals for single species fits of Ax330 Gαi1•GDP, Ax330 Gαi1:Ric-8A, and Alexa 488 β-ME adduct. (From Black et al. [1])

12.4.2 FCS Data Analysis and Results

Assuming fluorescence fluctuations arise from concentration changes within the confocal volume and are described by $\partial F(t) \equiv F(t) - \langle F(t) \rangle$, following the treatment of Schwille et al. [4, 12], the normalized fluorescence autocorrelation function $G_{ii}(\tau)$, with lag time τ, is defined as:

$$G_{ii}(\tau) = \frac{\langle \partial F_i(t) \cdot \partial F_i(t+\tau) \rangle}{< F_i(t) >^2}. \tag{12.8}$$

A three-dimensional diffusion autocorrelation function for species i can be describe as:

$$G_{ii}(\tau) = \sum_{i=1}^{n} \rho_i \left(1 + \frac{\tau}{\tau_i}\right)^{-1} \left(1 + \frac{\tau}{\tau_i \kappa^2}\right)^{-\frac{1}{2}}, \tag{12.9}$$

where $\sum_{i=1}^{n} \rho_i = 1/\langle N \rangle$ is the inverse of the average number of molecules inside the effective observation volume, $V_{eff} = \pi^{3/2} \omega_0^2 z_0$, and $\tau_i = \omega_0^2 / 4D_i$ is defined as the average lateral diffusion time for a molecule of species i moving through V_{eff}; $\kappa = z_0/\omega_0$ is the ratio of vertical to horizontal radii defining the ellipticity of V_{eff}. Through calibration of V_{eff} with a known standard, the translational diffusion

coefficient (D_i) can be derived from the characteristic decay time, τ_i. The ellipticity of $G_{ii}(\tau)$, can be significantly distorted by intersystem crossing of the dye from the singlet excited state to the triplet state, APD shot-noise and after-pulsing, all of which must be accounted for. To remedy this, a triplet-state "character" τ_T, is incorporated in $G_{ii}(\tau)$:

$$G_{ii}(\tau) = \left(1 - T + Te^{-\frac{\tau}{\tau_T}}\right) \sum_{i=1}^{n} \rho_i \left(1 + \frac{\tau}{\tau_i}\right)^{-1} \left(1 + \frac{\tau}{\tau_i \kappa^2}\right)^{-\frac{1}{2}} \tag{12.10}$$

with $\sum_{i=1}^{n} \rho_i = 1/[\langle N \rangle (1 - T)]$, and a lifetime gating filter is applied, eliminating the need for cross-correlation [24].

The Stokes-Einstein equation [8],

$$D_{translational} = \frac{k_B T}{6\eta\pi r}, \tag{12.11}$$

and Stokes-Einstein-Debye equation [6],

$$D_{rotational} = \frac{k_B T}{6\eta \left(\frac{4}{3}\pi r^3\right)}, \tag{12.12}$$

were used to relate translational diffusion to rotational diffusion such that

$$D_{rotational} = D_{translational} \frac{3}{4r^2}, \tag{12.13}$$

where k_B is Boltzmann's constant, T is temperature, η is the viscosity of the medium and r is the hydrodynamic radius of a spherical rotating body.

The rotational correlation time (τ_R) is related to $D_{rotational}$ by:

$$\tau_R = \frac{1}{6D_{rotational}} \quad . \tag{12.14}$$

The translational diffusion coefficient for Gαi1•GDP and GTPγS determined by this study was 97 (−6, 7) μm^2 s^{-1} and 92 (−5, 6) μm^2 s^{-1}, respectively. The Gαi1:Ric-8A complex had a smaller diffusion coefficient of 65 (−5, 6) μm^2 s^{-1} (95% confidence limits are in parentheses), as expected for a complex with larger molecular mass and surface area. Using the Stokes-Einstein-Debye relations [6], these values translate to global-rotational correlation times of 15 (−1, 2) ns and 53 (−4, 4) ns for nucleotide- and Ric-8A-bound states, respectively, at 25 °C.

12.5 Time-Resolved Fluorescence Anisotropy

12.5.1 TRFA Data Collection

TRFA decay measurements were carried out as described [5]. A 468-nm laser diode (LDH-P-C-470; PicoQuant GmbH, Berlin) was used for excitation at a repetition rate of 10 MHz. Vertical excitation-vertical emission (VV) and vertical excitation-horizontal emission (VH) were selected by a beam-splitting Glan-Thompson polarizer (Karl-Lambrecht, Chicago, IL), allowing simultaneous collection of both decay curves. Emission was isolated by 525/50-nm (Chroma Technology Corp., Bellows Falls, VT) band-pass filters, and IBH model TBX-04 photomultipliers (Glasgow, Scotland) were used for time-correlated single-photon counting (TCSPC). VV and VH decay curves were collected for equal times using a PRT 400 router and TimeHarp 200 PCI board (PicoQuant GmbH, Berlin) until $4x10^4$ counts (timing resolution of 35 ps/channel) were reached at the maximum of the VV curve. The instrument response function (IRF) was determined using colloidal silica.

12.5.2 TRFA Data Analysis and Results

Vertical and horizontal decay curves (V and H in Fig. 12.4, below), using vertical excitation, were fit globally using iterative re-convolution by trial decay functions.

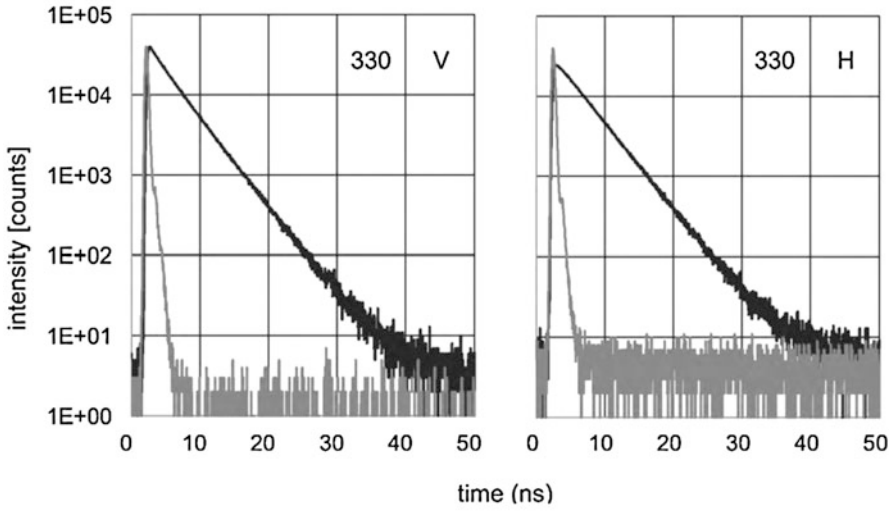

Fig. 12.4 Anisotropy decay data: Ax330 Gαi1•GDP at 25 °C. The left-hand and right-hand plots show the parallel (V) and perpendicular (H) decay curves (black) and IRFs (grey) for the anisotropy decay (35 ps/channel). (From Black et al. [1])

The anisotropy decay was fit as sums of exponentials according to the following relationships [8]:

$$I_{VV}(t) = G\frac{1}{3}\sum_{i=1}^{n}\alpha_i e^{-t/\tau_i}\left[1 + 2\sum_{j=1}^{5}\beta_j e^{-t/\phi_j}\right] \tag{12.15a}$$

$$I_{VH}(t) = \frac{1}{3}\sum_{i=1}^{n}\alpha_i e^{-t/\tau_i}\left[1 - \sum_{j=1}^{5}\beta_j e^{-t/\phi_j}\right] \tag{12.15b}$$

where α_i and β_j are the amplitudes of the lifetime intensity decay components, τ_i, and the rotational correlation time components, ϕ_j, respectively. The sum of β_j for all anisotropy components is equal to the time-zero limiting anisotropy, r_0. The difference in the photon detection efficiencies of the V and H channels was determined by collecting decay curves using horizontal excitation (i.e., HV and HH) and integration of these decay curves provided $G = \int I_{HV}dt / \int I_{HH}dt$, the correction factor used in Eqs. 12.15a, b. The χ^2 statistic was used to minimize the residual difference between the data and the model fit, and the autocorrelation of the residuals was used to visually inspect the goodness of the fit. The 95% confidence limits of the error in the fitting parameters was determined by using the support-plane method [25].

To demonstrate the effectiveness of independently determining the global rotational correlation time via FCS and fixing this parameter in the TRFA decay model, we will consider data for the α5, c-terminal Gαi1 Hexa I residue mutation, Ax330; the TRFA data are shown in Fig. 12.4.

Results for Ax330 Gαi1•GDP The left-hand column of Fig. 12.5, V1 and H1, shows residuals and autocorrelation of the residuals for fitting the above anisotropy decay data with a single rotational correlation time, which yields a value of 6.59 ns, r_0 of 0.202, and $\chi^2 = 2.91$; the non-randomly distributed residuals and autocorrelation function indicate that a single rotational correlation time model yields a poor fit. Statistically satisfactory fits have χ^2 values close to 1.0; the residuals and autocorrelation function both will be randomly distributed about zero throughout the time range. This is demonstrated in the middle column of Fig. 12.5, V2 and H2, for a fit with two unconstrained rotational correlation times. When data for all other Gαi1 complexes were fit with a single rotational correlation time, high χ^2 values and non-random residuals were obtained, indicating that in all cases the Alexa 488 probe is reporting complex dynamics.

The middle column, V2 and H2, shows residuals and their autocorrelation when fitting two unconstrained rotational correlation times. This fit yields short and long correlation times of 0.93 (−0.19, 0.23) ns, $\beta_{short} = 0.127$ (−0.007, 0.007) and 15.31 (−2.15, 3.09) ns, $\beta_{long} = 0.131$ (−0.006, 0.005) with r_0 of 0.258, $\chi^2 = 1.13$. Fixing the long correlation time at 15 ns, the average value calculated from FCS data (see

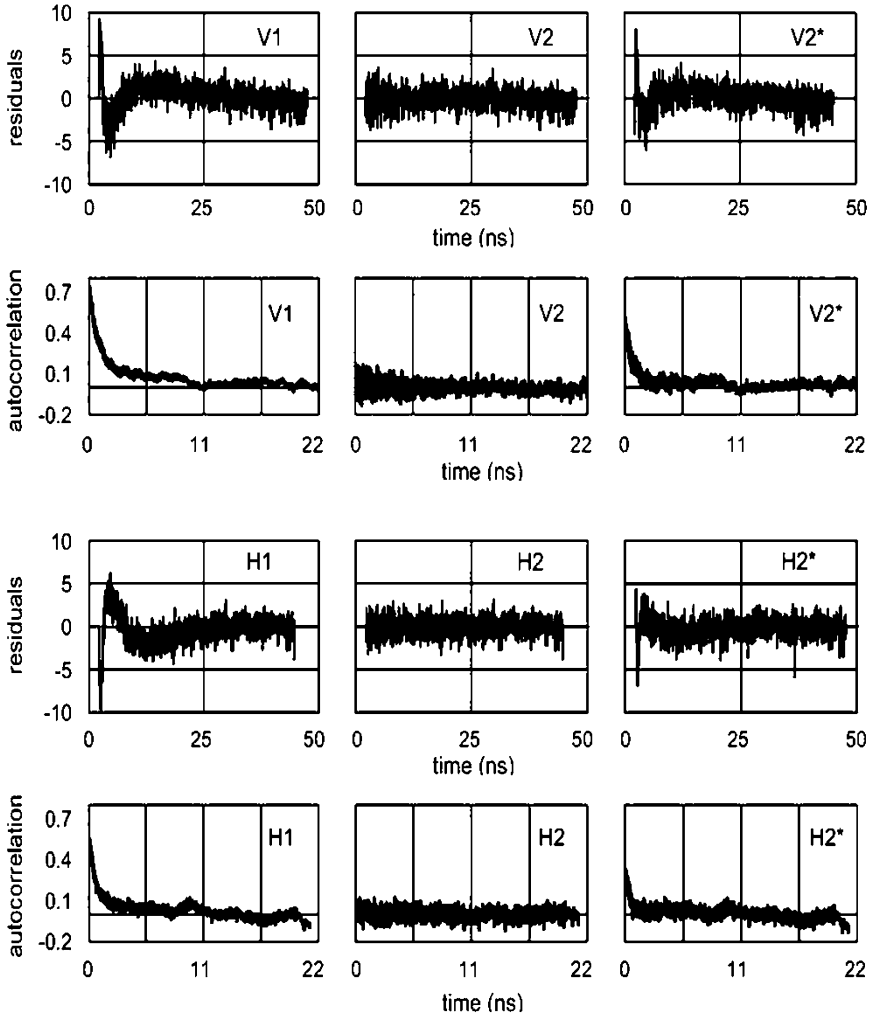

Fig. 12.5 The residuals and their autocorrelation for fits of the Ax330 Gαi1•GDP anisotropy decay data. (From Black et al. [1])

below), yields the same parameters and same χ^2 with equivalent residuals and autocorrelation function.

The right-hand column, V2* and H2*, shows residuals and their autocorrelation for two rotational correlation times when the long and short correlation times are fixed at 15 and 2.31 ns, respectively; the value for the short correlation time was obtained from analysis of the anisotropy decay data of the Ax330 Gαi1:Ric-8A complex with the long correlation time fixed at 53 ns, described below. The sum of β_j gave an r_0 of 0.222 and $\chi^2 = 1.73$, indicating that a short correlation time of 2.31 ns does not fit the anisotropy decay data for the GDP complex.

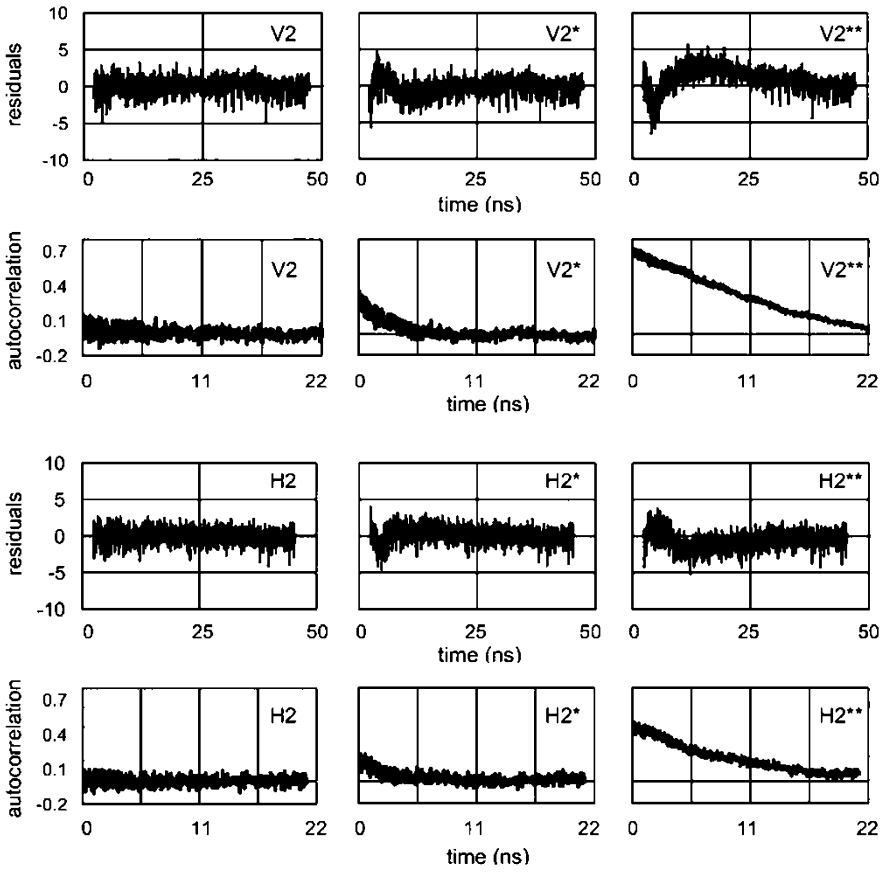

Fig. 12.6 The residuals and their autocorrelation for fits of the Ax330 Gαi1:Ric-8A anisotropy decay data. (From Black et al. [1])

Results for Ax330 Gαi1:Ric-8A Results for the Ric-8A complex are shown in Fig. 12.6 for three different models, each with two rotational correlation times. The left-hand column, V2 and H2, shows the residuals and autocorrelation for an unrestricted analysis, which yielded a short correlation time of 2.05 (−0.39, 0.48) ns, $\beta_{short} = 0.077$ (−0.008, 0.009), a long correlation time of 47.8 (−7.1, 11.7) ns, $\beta_{long} = 0.225$ (−0.011, 0.008) with r_0 of 0.302, and $\chi^2 = 1.08$. When the long correlation time is fixed at 53 ns, which is the average value for the global rotation of the Ric-8A complexes calculated from the translational diffusion coefficient determined from FCS data (see below), the short correlation time increases slightly to 2.31 (−0.22, 0.25) ns with $\beta_{short} = 0.082$ (−0.003, 0.003) and $\beta_{long} = 0.219$, yielding a similar r_0 of 0.301, the same χ^2 of 1.08, and similar residuals and autocorrelation.

The middle column, V2* and H2*, shows residuals and autocorrelation for two rotational correlation times when the shorter component is fixed at 0.93 ns, a value obtained from analysis of the Ax330 Gαi1•GDP complex (above), and the longer component is fixed at 53 ns, the value obtained from the FCS data. This gave r_0 of 0.323 and $\chi^2 = 1.37$. The nonrandom residuals and autocorrelation at early times in the decay (within 5 ns) of both V2* and H2* indicate that a short correlation time fixed at 0.93 ns (about half the value of that obtained from either fit described in the preceding analysis) does not fit the anisotropy decay of the Ric-8A complex.

The right-hand column, V2** and H2**, shows residuals and autocorrelation for two rotational correlation times when the long correlation time is fixed at 15 ns, the value obtained from FCS measurements used in analysis of the Ax330 Gαi1•GDP complex (above). This gave an r_0 of 0.294 with negligible contribution from a shorter correlation time, and $\chi^2 = 2.60$. Visual inspection of the residuals and their autocorrelation clearly shows that a long rotational correlation time of 15 ns does not fit the anisotropy decay of the Ax330 Gαi1:Ric-8A complex.

Local and global motions in Ax330 Gαi1•GDP and Ax330 Gαi1:Ric-8A Using fixed values for the global rotational correlation time of the GDP and Ric-8A complexes, derived from the FCS measurements, reduces the cross-correlation between the amplitudes and rotational time constants. In the case of the GDP complex, there are essentially no differences in the recovered parameters for the short and long rotational correlation times, but fixing the long correlation time does result in smaller error limits. In the case of the Ric-8A complex, however, the long rotational correlation time and its associated amplitude were strongly correlated in the unrestricted analysis of the TRFA data. As a result, both had large error limits; neither parameter was well defined. This is no surprise: considering the molecular weight of the Ric-8A complex, ~100 kDa, the expected mean global correlation time would be on the order of 50 nanoseconds, which is about two orders of magnitude slower than the timescale for the expected local motions and more than ten times slower than the mean fluorescence lifetime of the Alexa 488 probe. It is noteworthy that the FCS-determined value for the global rotational correlation time of the Ric-8A complex is 53 nanoseconds, which is longer than that obtained from unrestricted analysis of the TRFA data.

The TRFA parameters reveal significant differences in the dynamics of the nucleotide and Ric-8A complexes. The Ax330 Gαi1•GDP TRFA parameters describing the motions of the Alexa 488 (C5) fluorophore yield an order parameter $S^2 = 0.48$ (−0.04, 0.04)—cone angle $\theta = 39°$ (−2°, 3°)—*with the short correlation time yielding,* $\phi_{local} = 1.1$ (−0.2, 0.2) nanoseconds with $r_0 = 0.26$ (−0.02, 0.02). Binding Ric-8A restricts the dynamics of the local motions as indicated by an order parameter $S^2 = 0.73$ (−0.06, 0.06)—cone angle $\theta = 26°$ (−1°, 1°)—*and the longer correlation time,* $\phi_{local} = 2.3$ (−0.5, 0.6) nanoseconds; the limiting anisotropy $r_0 = 0.30$ (−0.02, 0.02). The lower r_0 value of the GDP complex likely reflects unresolved picosecond timescale motions that are sufficiently damped in the Ric-8A complex to contribute to β_{short}.

12.6 Conclusion

The TRFA of fluorescent probes covalently linked to single Cys-mutations introduced at different sites of interest within Gαi1 display two exponential decay components, one in the time range of 0.5 to about 3 ns and the other in the time range expected for global motion of the different complexes. To facilitate comparable resolution of the effects of ligand-binding on the global and local dynamics, the global rotational correlation time was calculated from the translational diffusion coefficient, determined by FCS, and the value was used as a fixed parameter in the analysis of the multi-exponential anisotropy decay model. This procedure limits cross-correlation between the local and global components in the TRFA decay and leads to a significantly more accurate and precise comparison of the local dynamics of the relative Gαi1 binding states, which can be described by the order parameter, S^2.

Acknowledgments The authors are grateful for support from National Institutes of Health Grant R01GM105993 (S.R. Sprang). Fluorescence measurements and analyses were performed in the BioSpectroscopy Core Research Laboratory at the University of Montana, which is operated with support from NIH Centers of Biomedical Research Excellence (CoBRE) Award P20GM103546 to the Center for Biomolecular Structure and Dynamics and from the Vice President of Research and Creative Scholarship at the University of Montana. The authors also acknowledge helpful discussions with colleagues Stephen R. Sprang and Celestine Thomas as well as technical assistance from Michelle Terwilliger.

References

1. Black LA, Thomas CJ, Nix GN, Terwilliger MC, Sprang SR, Ross JBA (2016) Nanosecond dynamics of Galphai1 bound to nucleotides or Ric-8A, a Galpha chaperone with GEF activity. Biophys J 111:722–731
2. Waxman E, Laws WR, Laue TM, Nemerson Y, Ross JBA (1993) Human factor VIIa and its complex with soluble tissue factor: evaluation of asymmetry and conformational dynamics by ultracentrifugation and fluorescence anisotropy decay methods. Biochemistry 32:3005–3012
3. Joo C, Balci H, Ishitsuka Y, Buranachai C, Ha T (2008) Advances in single-molecule fluorescence methods for molecular biology. Annu Rev Biochem 77:51–76
4. Medina MA, Schwille P (2002) Fluorescence correlation spectroscopy for the detection and study of single molecules in biology. BioEssays 24:758–764
5. Minazzo AS, Darlington RC, Ross JBA (2009) Loop dynamics of the extracellular domain of human tissue factor and activation of factor VIIa. Biophys J 96:681–692
6. Yao S, Babon JJ, Norton RS (2008) Protein effective rotational correlation times from translational self-diffusion coefficients measured by PFG-NMR. Biophys Chem 136:145–151
7. Yguerabide J, Epstein HF, Stryer L (1970) Segmental flexibility in an antibody molecule. J Mol Biol 51:573–590
8. Lakowicz JR (2006) Principles of fluorescence spectroscopy, 3rd edn. Springer, New York
9. Yguerabide J (1972) Nanosecond fluorescence spectroscopy of macromolecules. Methods Enzymol 26:498–578
10. Wahl P (1977) Statistical accuracy of rotational correlation times determined by the photocounting pulse fluorimetry. Chem Phys 22:245–256

11. Dale RE, Chen LA, Brand L (1977) Rotational relaxation of the "microviscosity" probe diphenylhexatriene in paraffin oil and egg lecithin vesicles. J Biol Chem 252:7500–7510
12. Ries J, Schwille P (2012) Fluorescence correlation spectroscopy. BioEssays 34:361–368
13. Belford GG, Belford RL, Weber G (1972) Dynamics of fluorescence polarization in macromolecules. Proc Natl Acad Sci USA 69:1392–1393
14. Chuang TJ, Eisenthal KB (1972) Theory of fluorescence depolarization by anisotropic rotational diffusion. J Chem Phys 57:5094–5097
15. Rigler R, Ehrenberg M (1976) Fluorescence relaxation spectroscopy in the analysis of macromolecular structure and motion. Q Rev Biophys 9:1–19
16. Barkley MD, Kowalczyk AA, Brand L (1981) Fluorescence decay studies of anisotropic rotations of small molecules. J Chem Phys 75:3581–3593
17. Small EW, Isenberg I (1977) Hydrodynamic properties of a rigid molecule: rotational and linear diffusion and fluorescence anisotropy. Biopolymers 16:1907–1928
18. Kinosita K Jr, Ikegami A, Kawato S (1982) On the wobbling-in-cone analysis of fluorescence anisotropy decay. Biophys J 37:461–464
19. Cheng CY, Jarymowycz VA, Cortajarena AL, Regan L, Stone MJ (2006) Repeat motions and backbone flexibility in designed proteins with different numbers of identical consensus tetratricopeptide repeats. Biochemistry 45:12175–12183
20. Medkova M, Preininger AM, Yu NJ, Hubbell WL, Hamm HE (2002) Conformational changes in the amino-terminal helix of the G protein alpha(i1) following dissociation from Gbetagamma subunit and activation. Biochemistry 41:9962–9972
21. Dertinger T, Loman A, Ewers B, Muller CB, Kramer B, Enderlein J (2008) The optics and performance of dual-focus fluorescence correlation spectroscopy. Opt Express 16:14353–14368
22. Nitsche JM, Chang HC, Weber PA, Nicholson BJ (2004) A transient diffusion model yields unitary gap junctional permeabilities from images of cell-to-cell fluorescent dye transfer between Xenopus oocytes. Biophys J 86:2058–2077
23. Petrasek Z, Schwille P (2008) Precise measurement of diffusion coefficients using scanning fluorescence correlation spectroscopy. Biophys J 94:1437–1448
24. Bohmer M, Wahl M, Rahn HJ, Erdmann R, Enderlein J (2002) Time-resolved fluorescence correlation spectroscopy. Chem Phys Lett 353:439–445
25. Straume M, Frasier-Cadoret SG, Johnson ML (1991) Least-squares analysis of fluorescence data. In: Lakowicz JR (ed) Topics in fluorescence spectroscopy. Kluwer Academic Publishers, New York, pp 177–240